Measurement of absolute line intensities in the $\nu 5$ - $\nu 4$ band of 12C2H2 using SOLEIL synchrotron far infrared AILES beamline

David Jacquemart, Laura Gomez, Nelly Lacome, Jean-Yves Mandin, Olivier Pirali, Pascale Roy

Measurement of absolute line intensities in the $\nu_5 - \nu_4$ band of $^{12}C_2H_2$ using SOLEIL synchrotron far infrared AILES beamline

D. Jacquemart [a,b,*], L. Gomez [a,b,‡], N. Lacome [a,b], J.-Y. Mandin [c,d], O. Pirali[e,f], P. Roy[e]

[a] *UPMC Univ Paris 06, UMR 7075, Laboratoire de Dynamique Interactions et Réactivité, Case courrier 49, Bât. F 74, 4, place Jussieu, 75252 Paris Cedex 05, France*

[b] *CNRS, UMR 7075, Laboratoire de Dynamique Interactions et Réactivité, Case courrier 49, Bât. F 74, 4, place Jussieu, 75252 Paris Cedex 05, France*

[c] *UPMC Univ Paris 06, UMR 7092, Laboratoire de Physique Moléculaire pour l'Atmosphère et l'Astrophysique, Case courrier 76, 4, place Jussieu, 75252 Paris Cedex 05, France*

[d] *CNRS, UMR 7092, Laboratoire de Physique Moléculaire pour l'Atmosphère et l'Astrophysique, Case courrier 76, 4, place Jussieu, 75252 Paris Cedex 05, France*

[e] *Synchrotron SOLEIL, L'Orme des Merisiers, Saint-Aubin, 91192 Gif-sur-Yvette Cedex, France*

[f] *Laboratoire de Photophysique Moléculaire, UPR3361 du CNRS, Université de Paris-Sud, Bâtiment 350, 91405 Orsay cedex, France*

Received 2009

[*] Corresponding author. Tel.: + 33-1-44-27-36-82; fax: + 33-1-44-27-30-21.
E-mail address: david.jacquemart@upmc.fr (D. Jacquemart).
[‡] Current address: *Groupe de Spectrométrie Moléculaire et Atmosphérique, CNRS, UMR 6089, Université de Reims-Champagne-Ardenne, Faculté des Sciences,BP 1039, 51687 Reims Cedex 2, France*
.

Abstract

Absolute intensities of about 120 lines of the $^{12}C_2H_2$ molecule are reported for the $\nu_4 - \nu_5$ band between 65 and 192 cm^{-1}, with an average accuracy of 5%. Vibrational transition dipole moment squared values and empirical Herman-Wallis coefficients are obtained allowing modelling the rotational dependence of the transition dipole moment squared. Special care is taken to accurately determine an apparatus function for the Bruker IFS 125-HR coupled to the synchrotron SOLEIL far infrared AILES beamline in order to minimize its effects on the line parameter retrieval.

Keywords: Acetylene; Infrared; Vibration-rotation; Line intensities; Databases; SOLEIL synchrotron; Apparatus function.

1. Introduction

The infrared spectroscopy of the acetylene molecule C_2H_2 is important for atmospheric, planetary, and astrophysical applications (prebiotic molecule), as well as for industrial applications. This molecule is present as a trace constituent in the upper atmosphere of giant planets and satellites such as Titan where it results from methane photodissociation and has been detected for example in spectra recorded with the infrared radiometer-infrared spectrometer (IRIS) instrument on board Voyager 1 and 2 [1]. Acetylene was also observed in the circumstellar shell of cool carbon stars such as IRC+10216 [2], and in interstellar clouds. A few years ago, it was possible to deduce the stratospheric distribution of acetylene in Uranus from spectra obtained with the Infrared Space Observatory instruments (ISO) [3]. Recent and future instruments as e.g. SPITZER [4,5], ALMA [6], or HERSCHEL [7] will operate in the FIR spectral region where only very few line intensities have been measured.

The present data have been obtained using the AILES-A (Advanced Infrared Line Exploited for Spectroscopy) beamline of SOLEIL synchrotron. This beamline located at the third generation Synchrotron Radiation source SOLEIL allows high resolution spectroscopic measurements of molecules in the entire infrared and THz range. The performances concerning flux, spectral range and stability can be particularly advantageous for high resolution FTIR spectrometer as the beamline optics permits the entire source to be used without aperture stop (entrance iris), even for measurements at highest-resolution of ~0.1 μeV (10^{-3} cm^{-1}). For this study, the spectral region (50-600 cm^{-1}) was exploited. This frequency range comprises two spectral regions of the acetylene absorption, corresponding to the $\Delta P = 0$ and 1 sequence of vibrational transitions [8], P being a pseudo-quantum number equals to $5v_1 + 3v_2 + 5v_3 + v_4 + v_5$, where v_1, v_2, v_3, v_4, and v_5 are the quantum numbers associated with the normal modes of vibration of the molecule in the ground electronic state. Extensive work on this spectral region has been performed by Kabbadj et al [9] who assigned vibro-rotational lines for 5 hot bands around 100 cm^{-1} ($\Delta P = 0$) and 5 hot bands around 500 cm^{-1} ($\Delta P = 1$). Among them, line intensities have been studied only for some lines of the $\nu_5^1 - \nu_4^1$ intense band, by Robert et al [10]. The superscript in the notation of this band refer to $\ell = |\ell_4 + \ell_5|$, ℓ_t being the vibrational angular momentum quantum number associated with the degenerated bending mode t. From the measurement of these line intensities, the vibrational transition dipole moment squared of the $\nu_5^1 - \nu_4^1$ band has been deduced with an accuracy expected to be close to 20% in Ref. [10]. A synthetic spectrum of this band was then calculated and included in the Cologne Database for Molecular Spectroscopy (CDMS) [11]

(273 lines from 1 to 242 cm^{-1}, namely up to *J* equal 51 for various branches) with obvious astrophysical applications for the Herschel Space Observatory [12] but also for all instruments performing detection in this spectral range.

The goal of this work was to measure absolute line intensities at room temperature in the 50-600 cm^{-1} spectral region for all the bands observed in Ref. [9] in the two spectral regions of the acetylene absorption. To perform intensity measurements, several spectra have been recorded with a Fourier transform spectrometer Bruker IFS 125-HR. The SOLEIL synchrotron facility allows recording spectra with superior brilliance in the far infrared while providing an increased signal to noise ratio compared to classical sources. An important preliminary study on the apparatus function calculation and its effects on the line parameter retrieval was firstly performed. Taking into account the allowed beamtime, the experimental spectra have only been recorded with a single absorption path of around 10 meters. Then, line intensities could be measured only in the $\nu_5^1 - \nu_4^1$ band. For a complete and accurate analysis of the other bands, a larger absorption path will be required (around 100 m). In this work, a set of 120 absolute line intensities has been obtained with an average accuracy of 5%, and transition dipole moment squared values have been deduced. The next section of the paper will be devoted to the experimental conditions, to the analysis of the apparatus function and to its effects on the line parameter retrieval. The present results concerning line intensity measurements will be presented in Section 3, together with a comparison of transition dipole moments squared obtained in this work and those of Robert et al [10].

2. Experimental conditions and preliminary studies

2.1. Experimental conditions

Six spectra have been recorded with the rapid scan Bruker IFS 125 HR interferometer coupled to the far infrared beamline AILES of the SOLEIL synchrotron. This beamline utilizes infrared synchrotron radiation from both edge emission [13] and constant field synchrotron source. The far infrared synchrotron emission is extracted and transported under vacuum in AILES beamline and is focused on the entrance aperture of the high resolution interferometer. The beam spot appears to be highly symmetric in the horizontal plane, while large asymmetry is observed along the vertical axe. This shape showing a peak like distribution from the edge emission and the flat distribution of the constant field is in excellent agreement with the ray tracing calculations (SRW) at this wavelength [14]. This narrow profile explains how the AILES beam is well adapted for high resolution measurements. Indeed, with this

distribution, no iris is needed even for the highest resolution measurements. For lower energy, the natural cone opens up as described in [15], and remains compatible with high resolution as the maximum iris size increases for decreasing energy. This advantage turns out to be particularly valuable when combining the high resolution interferometer with a multipass cell (White type configuration).

For the present measurements, the Bruker IFS 125 is equipped with a 6 µm Mylar beam splitter, and a 4.2 K Si-bolometer detector. Experimental conditions are gathered in Table 1. An optical filter covering the spectral region between 50 and 600 cm^{-1} was employed. The whole optical path is under vacuum and a metal multipass White-type cell (2.5-m base length) was aligned to provide a 10.14 ± 0.01 m absorption path length. The cell was equipped with 50 µm thick polypropylene windows. The temperature of the gas inside the cell has been obtained by averaging measurements performed in the room at different times, so that the uncertainty on the temperature has been estimated to be around ±1 K. Gas pressures were measured using two sets of full scale ranges MKS Baratrons (10- and 100-Torr manometers of 0.5% accuracy) and placed at both extremities of the cell. The deviation between the two sets of MKS Baratrons (one from the LADIR in Paris, the other from the AILES beamline) is within the 0.5% accuracy of the Baratrons. Each spectrum has been obtained by averaging about 300 records depending on the spectrum (see Table 1). When these spectra were recorded, reinjection of electron bunches occurred every 8 hours, thus special care was taken to remove corresponding scans for which extra spectral noises can be observed. The Fourier transform procedure used is the one included in the Bruker software OPUS package [16], selecting a Mertz phase error correction [17,18]. The signal to noise ratio of the average spectra depends on the wavenumber and is about 120 near the $\nu_5^1 - \nu_4^1$ band around 120 cm^{-1}. As it can be observed in Fig.1, an important irregular multiplicative channel spectrum is present on the spectra. This channel spectrum has been modelled locally as a background adjusted on a small spectral domain of around 0.020 cm^{-1} with a second order polynomial function. In this figure, intensity alternations characteristics of the $^{12}C_2H_2$ isotopologue are well observed in the two sub-branches expanding in opposite directions. Note that a spectrum recorded with the source turned off allowed verifying that the emission of the cell, detector, or optical filter could be neglected in our experimental configuration.

2.2. Preliminary study: wavenumber calibration and apparatus function

To deduce line parameters from the spectra, a multispectrum procedure was used following a method previously described [19]. In Fourier transform spectroscopy, when the source is limited by an iris, the apparatus function is determined by the maximum optical path depth, the optical weighting due to the through-put, and eventually the phase error [20,21]. The optical weighting of the interferogram can be calculated as follows [22]:

$$P_{opt}(\Delta) = \left| \frac{\sin\left(\frac{\sigma_0 \pi R^2 \Delta}{2f^2}\right)}{\frac{\sigma_0 \pi R^2 \Delta}{2f^2}} \right|, \quad (1)$$

where f is the collimator focal length, σ_0 is the analyzed wavenumbers and R the iris radius. In the case of the synchrotron beam, R is the radius of the beam.

Usually, the value of R from Eq. (1) is different from the nominal measured value of the iris radius, so that an effective value is adjusted using the fitting procedure developed in Ref. [19]. In the case of the particular beam extracted by AILES, the full synchrotron beam is injected, and the beam size depends on the wavenumber in contrast with classical sources. The spatial distribution of the photons delivered by AILES has been modelled [15] using the Ray Tracing software SOLEMIO [23] and SRW [14]: the spatial distribution at various wavenumbers appears not to be truly Gaussian and the size of the beam (given by an effective diameter) has been estimated to be around 7 mm at 10 cm^{-1}, 2.5 mm at 100 cm^{-1}, and 0.8 mm at 1000 cm^{-1}. In addition, the profile at 800 cm^{-1} was confirmed experimentally [24]. In the following, the beam has been considered as if it was limited by an iris of radius R to be determined as a fitted parameter. In some cases, depending on the size of the beam, the focal of the collimator, the wavenumber, and the resolution, the effect of the optical weighting is important and can not be neglected. It is the case of the spectra obtained in this work, since the full width at half maximum (FWHM) of the apparatus function (between 0.001 and 0.002 cm^{-1} depending on the spectrum) is the same order of magnitude as the FWHM of the lines (between 0.0002 and 0.004 cm^{-1} depending on the spectrum), so that distortions due to the apparatus function and its apodization due to the through-put can not be neglected.

In order to better estimate these effects, isolated lines of both acetylene and water (present as traces in the cell and/or in the interferometer) have been selected at various wavenumbers and their intensities were fitted letting free the effective beam radius parameter. This preliminary study allowed firstly, to estimate an effective value of the size of the beam, but also to perform an absolute wavenumber calibration using as reference the absolute

wavenumbers given in the HITRAN database [25] for 45 isolated water vapour transitions between 70 and 500 cm^{-1} (line positions coming from Ref. [26]). This wavenumber calibration has been performed for spectra 1 and 2, and is almost identical for both spectra: $<\sigma_{obs}-\sigma_{HITRAN}>=(-0.15 \pm 0.21)\times10^{-3}$ cm^{-1} for spectrum 1 compared with $(-0.13 \pm 0.18)\times10^{-3}$ cm^{-1} for spectrum 2, with 1 SD after the ± sign. Consequently, an average constant calibration difference of -0.14×10^{-3} cm^{-1} has been applied to all spectra. For spectra 1-4 (see Table 1), the FWHM of the apparatus function is preponderant compared with the FWHM due to collisions or to the Doppler effect, so that the effect of the optical weighting due to the through-put can be adjusted with more accuracy on spectra 1-4 than on spectra 5-6. Results of the effective radius of the beam (R_{eff}) are presented on Fig. 2 together with the values estimated by the SOLEMIO and SRW softwares. As can be observed, the adjustments of water and acetylene transitions give equivalent results for R_{eff}, even if the dispersion of these results appears quite large. The decreasing of the size of the beam with increasing wavenumber is in agreement with predictions using SOLEMIO and SRW models. However, the size of the beam estimated through acetylene and water lines is slightly larger than this estimated by the SOLEMIO and SRW models. The effect of the radius of the beam has non negligible consequences on the line parameter retrieval, except when the apparatus function can be negligible, i.e. when the width of the apparatus function is much smaller than the line width due to collisions and Doppler effect, or when the optical weighting of interferogram can be neglected, i.e. $P_{opt}(\Delta_{max}) \approx 1$, in Eq. (1). In this work, these effects can not be neglected. Consequences on line intensities have been estimated by fitting acetylene lines using different values of the beam radius. Since only the $\nu_5^1 - \nu_4^1$ band is concerned in this work, the spectral range under study is between 65 and 192 cm^{-1}, and in this spectral range the variation of R_{eff} has been estimated using a straight line model:

$$R_{eff} = 2.27(9) - 4.4(7).10^{-3}\times \sigma_0 \quad \text{in mm,} \qquad (2)$$

where σ_0 is the wavenumber in cm^{-1}, and digit between parentheses is 1 SD in unit of the last quoted digit.

Three isolated acetylene lines (near 70, 100 and 180 cm^{-1}) have been chosen to evaluate the effect of various optical weightings on the calculated apparatus function and on the retrieved line parameters. For each line, three different values of R have been used in Eq. (1): the value obtained by the SOLEMIO and SRW models at 100 cm^{-1} (R = 1.25 mm), the R_{eff} values obtained from the straight line equation and the value of R = 0 mm when one neglects

the optical weighting. The optical weighting affects both the retrieved line intensity and self-broadening coefficients and we checked that when using R_{eff} values the self-broadening coefficients converged to better values (i.e. closer than those of the literature [27,28]) than when using the default value of 1.25 mm. However, due to the relatively low pressures (see Table 1), the measurement of line intensities have been performed fixing the self-broadening coefficients to the values given in HITRAN [25] and coming from Refs. [27,28]. The results are presented in Table 2, and the apparatus functions are plotted on Fig. 3. As can be observed on Fig.3, the apodization of the apparatus function depends not only on R, but also on the wavenumber, since the optical weighting is more important at higher wavenumbers. Therefore, the effect on the line intensity is larger at higher wavenumbers (see results in Table 2 obtained by the multispectrum fitting procedure), even for quite close values of R (1.25 compared with 1.48 mm). Note that the effect on the line positions is very weak (a few 10^{-5} cm^{-1}) and can be neglected in our study. Consequences on line intensities are not at all negligible since they can reach about 3.5%, which is large for absolute line intensity studies. An example of multispectrum fitting is presented on Fig. 4 for the R_{ff} (26) line located around 181.5 cm^{-1}. In this figure, the residuals of the fits obtained with various optical weightings are given. As can be observed, the best residuals are obtained when using R = 1.48 mm, the effective value obtained by Eq. (2). Note that the line shapes in spectra 4 and 5 are less affected by the use of different optical weightings, because of the higher pressures (see Table 1) leading to larger line widths. If one uses a single spectrum fitting procedure [19], the effect on the line intensity may be much larger depending on the analyzed spectrum (see Table 3). First, one sees that when the pressure is increasing (from spectrum 1 to 5), the effects on the retrieved line intensity become less important since the collisional width is larger, so that the apparatus function has less effect on the observed line profile. Moreover, as shown in Tables 2 and 3, the optical weighting can strongly affect the line intensity when using a single spectrum fitting procedure. To conclude, when the width of the apparatus function is not negligible compared with the collisional or Doppler widths of the lines, one has to accurately calculate the optical weighting in order to take it into account if necessary, as usual in quantitative Fourier transform spectroscopy. In the case of the synchrotron beam, the adjustment of an effective parameter, R_{eff}, appeared an efficient way to accurately reproduce the apparatus function and line shapes, as can be seen on Figs. 3 and 4, and then to avoid non negligible systematic errors in the retrieved line intensities.

3. Results and discussion

Using the preliminary study (wavenumber calibration and determination of the apparatus function for this given set of spectra), the multispectrum fitting procedure has been used on spectra 1-5, fixing the self-broadening coefficients at the values of Ref. [25]. Notice, however, that other parameters may affect the determination of the apparatus function (optics slight misalignment, non linearity of the detector especially if a large frequency domain is probed simultaneously, S/N ratio…). Absolute line positions and intensities have been retrieved for 117 transitions involving the two sub-branches of the $\nu_5^1 - \nu_4^1$ band. The results are given in Table 4 together with the calculation performed by Robert et al [10] and available (file 026505) in the Cologne Database for Molecular Spectroscopy (CDMS). The comparison of the absolute wavenumbers is very good since the average difference between this work and the calculation of Ref. [10] is $(0.02 \pm 0.11)\times10^{-3}$ cm^{-1}. As far as the line intensities are concerned, let us recall that in Ref. [10], from the measurement of some line intensities, the vibrational transition dipole moment squared of the $\nu_5^1 - \nu_4^1$ band had been deduced ($|R|^2$ = 0.0026 debye^2) with an accuracy expected not to be better than 20%. A synthetic spectrum of this band had then been calculated by Robert et al (273 lines from 10 to 242 cm^{-1}, namely up to J equal 51 for various branches). We observe a good agreement for the P- and R-branches between our measured values and those calculated from Ref. [10] (average ratio this work/Ref. [10] equal to 1.001 ± 0.040), whereas a significant difference is observed for both the Q_{ef} and Q_{fe}-branches. These differences are increasing with J.

In order to understand these discrepancies, the transition dipole moments squared $|R|^2$ have been calculated from the line intensities measured in this work. For each line intensity $S(T_0)$ obtained from the multispectrum fitting procedure, in cm molecule^{-1} for pure $^{12}C_2H_2$ (i.e., for a sample containing 100% of $^{12}C_2H_2$) at the standard temperature T_0 = 296 K, we used the following formula to deduce the transition dipole moment squared $|R|^2$, in D^2 (1 debye = 3.33546×10^{-30} C m)

$$S(T_0) = (1/4\pi\varepsilon_0)\,(8\pi^3/3hc)\,[g''\nu_0/g_V\,Q(T_0)]\,|R|^2\,L(J,\ell)\,\exp(-hcE''/kT_0)\,[1-\exp(-hc\nu_0/kT_0)], \quad (3)$$

where $1/4\pi\varepsilon_0 = 10^{-36}$ erg cm^3 D^{-2}; h is Planck's constant equal to $6.6260755 \times 10^{-27}$ erg s (1 erg = 10^{-7} J); c is the speed of light in vacuum equal to $2.99792458 \times 10^{10}$ cm s^{-1}; g'' is the statistical weight due to nuclear spin of the lower level (1 for s-type levels and 3 for a-type levels); ν_0 is the transition wavenumber in cm^{-1}; g_V depends on the degeneracy of the levels

involved, with the convention g_V equals 2 when both upper and lower vibrational states are degenerated (this is the case for the studied band) and equals 1 otherwise; $Q(T_0)$ is the total partition function at temperature T_0, calculated from Fischer et al [29]; $L(J,\ell)$ is the Hönl-London factor; E'', in cm^{-1}, is the energy of the lower level taken from HITRAN [25]; k is Boltzmann's constant equal to 1.380658×10^{-16} erg K^{-1}. For P- and R-branches of the parallel band $\nu_5^1 - \nu_4^1$ ($\Delta\ell = 0$), the Hönl-London factor is taken as in Ref. [30]

$$L(J,\ell) = (J+1+\ell)\,(J+1-\ell) / (J+1) \text{ (for } R\text{-branch)}, \quad (4)$$

$$L(J,\ell) = (J+\ell)\,(J-\ell) / J \text{ (for } P\text{-branch)}. \quad (5)$$

In order to compare our $|R|^2$ values with those given in Ref. [10], the g_v factor in Eq. (3) had to be taken equal to 1 instead of 2. Thus, the transition dipole moment squared values are given in Table 4 and plotted versus m (m being equal to $-J$ for the P-branch, J in Q-branch, and $J+1$ in the R-branch) on Fig. 5. These values can be compared to 0.0026 debye^2 given in Ref. [10]. This constant value is in good agreement for the P- and R- branches, but the transition dipole moment squared values associated to Q-branches are clearly J-dependent and can not be reproduced by this constant value. To reproduce this rotational dependence, effective parameters can be deduced expanding $|R|^2$ for both P-, Q- and R-branches:

$$|R|^2 = |R_0|^2\,(1 + A_1^{PR}\, m + A_2^{PR}\, m^2)^2 \text{ (for } P\text{- and } R\text{-branches)}, \quad (6)$$

$$|R|^2 = |R_0|^2\,(1 + A_2^{Q}\, m^2)^2 \text{ (for } Q\text{-branch)}. \quad (7)$$

$|R_0|^2$ is the vibrational transition dipole moment squared, and A_1^{PR}, A_2^{PR}, and A_2^{Q} are the Herman-Wallis coefficient for both *e*-and *f*-branches. Since no significant discrepancies are observed between the two sub-branches, the transition dipole moment squared values of both branches have been fitted together using Eqs. (6,7) fixing A_1^{PR}, A_2^{PR} equal to 0 (no significant rotational dependence is observed for these branches). As a result (see Fig. 5) we found $|R_0|^2 = (0.00263 \pm 0.00002)$ D^2, and $A_2^{Q} = (-2.3 \pm 0.2)\times 10^{-3}$. The agreement between the $|R_0|^2$ value obtained in this work and the one given in Ref. [10] is very good (difference of 0.1%). The rotational dependence observed for the line intensities of the weak Q-branches of the $\nu_5^1 - \nu_4^1$ will be better reproduced using the A_2^{Q} value found in this work than using only the constant value of the transition dipole moment squared given in Ref. [10].

4. Conclusion

Absolute intensities have been measured for about 120 lines in the $\nu_5^1 - \nu_4^1$ band of the $^{12}C_2H_2$ spectrum around 100 cm^{-1}. A good agreement is observed with Ref. [10] for both line positions and intensities, except for the line intensities of the *Q*-branches for which a rotational dependence of the transition dipole moment squared has been observed and modelled. Special care has been taken in this work to characterize an apparatus function for this set of experiments. It has been shown that in some cases, the optical weighting could be a significant source of systematic error in the line intensity retrieval. As a conclusion for future uses of the SOLEIL-AILES beam light, if the experimental conditions are such that the apparatus function can not be neglected, it is strongly recommended to determine an effective value for the radius of the beam before performing absolute line intensity retrievals.

Acknowledgments:

We acknowledge SOLEIL for provision of synchrotron radiation facilities and we would like to thank J.-B. Brubach, M. Rouzières and D. Balcon for assistance in using beamline AILES-A.

References

[1] Rudd RP, Hall JC, Sparadlin GL. The voyager interstellar mission. Acta Astonautica 1997;40:383-96.

[2] Fonfría JP, Cernicharo J, Richter MJ, Lacy JH. A detailed analysis of the dust formation zone of IRC+10216 derived from MID-IR bands of C_2H_2 and HCN. Astrophysical Journal 2008;673;445-69.

[3] Kessler MF, Barr P. The Infrared Space Observatory (ISO). Infrared Physics & Technology 1994;35:211-20.

[4] Werner MW. The spitzer space telescope mission. Advances in Space Research 2005;36:1048-9.

[5] Matsuura M, Wood PR, Sloan GC, Zijlstra AA. Spitzer observations of acetylene bands in carbon-rich asymptotic giant branch stars in the Large Magellanic Cloud. Mon Not R Astron Soc 2006;371:415-20.

[6] Brown RL, Wild W, Cunningham C. ALMA-the Atacama Large Millimiter Array. Advances in Space Research 2004;34:555-9.

[7] Harwit M. The Herschel mission. Advances in Space Research 2004;34:568-72.

[8] El Idrissi MI, Liévin J, Campargue A, Herman M. The vibrational energy pattern in acetylene (IV): updated global vibration constants for $^{12}C_2H_2$. J Chem Phys 1999;110:2074-86.

[9] Kabbadj Y, Herman M, Di Lonardo G, Fusina L, Johns JWC. The bending energy levels of C_2H_2. J Mol Spectrosc 1991;150:535-65.

[10] Robert S, Herman M, Vander Auwera J, Di Lonardo G, Fusina L, Blanquet G, Lepere M, Fayt A. The bending vibrations in $^{12}C_2H_2$: global vibration-rotation analysis. Mol Phys 2007;105:559-68. Robert S, Herman M, Vander Auwera J, Di Lonardo G, Fusina L, Blanquet G, Lepere M, Fayt A. Erratum. Mol Phys 2009;105:13.

[11] Müller HSP, Schlöder F, Stutzki J, Winnewisser G. The Cologne Database for Molecular Spectroscopy, CDMS: a useful tool for astronomers and spectroscopists. J Mol Struct 2005; 742: 215-227.

[12] de Graauw T, Helmich FP. The Promises of the Herschel Space Observatory. ESA SP-460, 45 (July 2001).

[13] Roy P, Cestelli M, Marcouillé O, Paolone A, Giura P, Mathis YL, Gerschel A. Spectral distribution of infrared synchrotron radiation by an insertion device and its edges: A comparison between experimental and simulated specta. Phys. Rev. Lett. 2000;84:483.

[14] Chubar O, Elleaume P. Accurate and efficient computation of synchrotron radiation in the near field region, in: Proceedings of the EPAC 98 Conference, 22–26 June, 1998, pp.1177–1179.

[15] Roy P, Rouzières M, Qi Z, Chubar O. The AILES Infrared Beamline on the third generation Synchrotron Radiation Facility SOLEIL. Infrared Physics & Technology 2006, 49:139-146.

[16] Wartewig S. IR and Raman Spectroscopy: Fundamental Processing. Weinheim: Wiley-VCH; 2003.

[17] Mertz L. Transformations in Optics. New York: Wiley; 1965.

[18] Griffiths PR, deHaseth JA. Fourier Transform Infrared Spectrometry. New York: Wiley; 1986.

[19] Jacquemart D, Mandin JY, Dana V, Picqué N, Guelachvili G. A multispectrum fitting procedure to deduce molecular line parameters. Application to the 3–0 band of $^{12}C^{16}O$. Eur Phys J D 2001;14:55-69.

[20] Dana V, Mandin JY. New improvements in the determination of line parameters from FTS data. JQSRT 1992;48:725-31.

[21] Dana V, Mandin JY, Hamdouni A. Phase errors on interferograms: influence on the determination of positions, intensities, and widths of lines in the infrared. Appl Opt 1992;31:1937-41.

[22] Guelachvili G. Distorsions in Fourier Spectra and diagnosis. *In* Vanasse GA, editor. Spectrometric techniques. Vol. II. New York: Academic Press, 1981. pp. 1-62.

[23] Lagarde B, Polack F. SOLEMIO Software, private communication.

[24] Brubach JB, Manceron L, Rouzières M, Pirali O, Balcon D, Kwabia Tchana F, Boudon V, Tudorie M, Huet Th, Cuisset A, Roy P. Performance of the AILES THz-Infrared beamline on SOLEIL for High resolution spectroscopy. AIP Conference Proceedings, 2009, in press.

[25] Rothman LS, Gordon IE, Barbe A, Chris Benner D, Bernath PF, Birk M, Brown LR, Boudon V, Champion JP, Chance K, Coudert LH, Dana V, Fally S, Flaud JM, Gamache RR, Goldman A, Jacquemart D, Lacome N, Mandin JY, Massie ST, Mikhailenko S, Orphal J, Perevalov V, Perrin A, Rinsland CP, Šimečková M, Smith MAH, Tashkun S, Tennyson J, Toth A, Vandaele AC, Vander Auwera J. The HITRAN 2008 Molecular Spectroscopic Database. JQSRT 2009;110:533-572.

[26] Lanquetin R, Coudert LH, Camy-Peyret C. High-lying rotational levels of water: an analysis of the energy of the five first vibrational states. J Mol Spectrosc 2001;206:83-103.

[27] Jacquemart D, Mandin JY, Dana V, Régalia-Jarlot L, Thomas X, Von der Heyden P. Multispectrum fitting measurements of line parameters for 5µm cold bands of acetylene. JQSRT 2002;75:397-422.

[28] Jacquemart D, Mandin JY, Dana V, Régalia-Jarlot L, Plateaux JJ, Décatoire D, Rothman LS. The spectrum of acetylene in the 5-µm region from new line parameter measurements. JQSRT 2003;76:237-267.

[29] Fischer J, Gamache RR, Goldman A, Rothman LS, Perrin A. Total internal partition sums for molecular species in the 2000 edition of the HITRAN database. JQSRT 2003;82:401-12.

[30] Vander Auwera J. Absolute intensities measurements in the ($\nu_4 + \nu_5$) band of $^{12}C_2H_2$: analysis of Herman-Wallis effects and forbidden transitions. J Mol Spectrosc 2000;201:143-50.

Captions of Tables

Table 1: Experimental conditions and characteristics of the spectra recorded using the rapid-scan interferometer of SOLEIL-AILES beamline.

Table 2: Effects of the size of the beam on the line positions and intensities, adjusted using a multispectrum procedure applied to spectra 1-5. The radius of the beam is fixed at 0 mm (no optical weighting), at 1.25 mm (estimated by the SOLEMIO and SRW models), or at values calculated by Eq. (2) and retained for the final study.

Table 3: Effect on line positions and intensities of the line $P_{ff}(7)$, when one applies a single spectrum fitting procedure to spectra 1-5, with the radius of the beam fixed at 0 mm (no optical weighting), at 1.25 mm (estimated by the SOLEMIO and SRW models), or at values calculated by Eq. (2) (retained effective values).

Table 4: Line parameters obtained for the $\nu_5{}^1 - \nu_4{}^1$ band of the $^{12}C_2H_2$ molecule and comparison with CDMS data. [a]

Captions of Figures

Figure 1: Overview of the weak *Q*-branches of the $\nu_5^1 - \nu_4^1$ band around 117.5 cm^{-1} on spectrum 4 (see Table1).

Figure 2: Estimation of the fitting parameter R_{eff}. The three stars are estimations of the size of the beam obtained using the SOLEMIO and SRW models at 10, 100 and 1000 cm^{-1}. The values of R_{eff} are indicated by solid symbols for acetylene transitions and by open symbols for water transitions. For spectrum 1, 2, 3, and 4, squares, triangles, circles, and upside down triangles have been respectively used.

Figure 3: Apparatus functions calculated around 80 (a), 100 (b) and 180 cm^{-1} (c), for various optical weightings. The continuous line represents the apparatus function without optical weighting (R=0 mm), whereas the dash and dot lines correspond respectively to an optical weighting using R=1.25 mm (estimated by the SOLEMIO and SRW models) and R deduced from Eq. (2) (see Table 2).

Figure 4: Residuals of a multispectrum fitting of the R_{ff} (26) line located around 181.5 cm^{-1}. The residuals are those obtained with no optical weighting (a), using R = 1.25 mm (b), and R = 1.48 mm (c). The experimental transmission is plotted. The sidelobes of the apparatus function are clearly visible and are well reproduced by the adjustments (differences can not be distinguished). The absence of systematic signature in the residuals of the body of the line (c), contrary to what is observed on plots (a) and (b), shows that our model of apparatus function is efficient and precise enough.

Figure 5: Transition dipole moment squared $|R|^2$ for the lines of the $\nu_5^1 - \nu_4^1$ band of acetylene $^{12}C_2H_2$. Solid symbols represent the P_{ee}, R_{ee} and Q_{fe} branches, whereas the open ones are for the P_{ff}, R_{ff} and Q_{ef} branches. Triangles represent both the *R*- and *P*-branches, whereas the square symbols are for the *Q*-branches. The continuous lines represent the calculation using Eqs. (6-7) together with the $|R_0|^2$ and A_2^Q values given in the text.

Table 1: Experimental conditions and characteristics of the spectra recorded using the rapid-scan interferometer of SOLEIL-AILES beamline.

Commercial sample (Air Liquide Alphagaz)	
Natural C_2H_2	97.760% of $^{12}C_2H_2$
Stated purity	99.55%
Total absorption path	10.29 m
Collimator focal length	418 mm
Beam size at focal point	see text

Spectrum number	Total pressure (hPa)	Temperature (K)	Bruker-resolution[a] (cm^{-1})	Number of co-added scans
1	0.598	300.1	0.002	300
2	1.204	300.0	0.002	266
3	2.450	300.2	0.002	299
4	4.886	300.0	0.003	336
5	9.798	299.6	0.003	292

[a] Bruker-resolution = $0.9/\Delta_{max}$., Δ_{max}.being the maximum optical path difference

Table 2: Effects of the size of the beam on the line positions and intensities, adjusted using a multispectrum procedure applied to spectra 1-5. The radius of the beam is fixed at 0 mm (no optical weighting), at 1.25 mm (estimated by the SOLEMIO and SRW models), or at values calculated by Eq. (2) and retained for the final study.

	R (mm)	Position (cm^{-1})	Line intensity ($cm\ molecule^{-1}$)	Ratio *
	0	70.51695(7)	$1.322(28)\ 10^{-23}$	--
P_{ff} (20)	1.25	70.51698(7)	$1.331(28)\ 10^{-23}$	1.007
	1.96	70.51697(7)	$1.355(28)\ 10^{-23}$	1.025
	0	100.95941(2)	$2.550(22)\ 10^{-23}$	--
P_{ff} (7)	1.25	100.95942(2)	$2.575(22)\ 10^{-23}$	1.010
	1.83	100.95945(2)	$2.649(22)\ 10^{-23}$	1.039
	0	181.52592(2)	$1.957(13)\ 10^{-23}$	--
R_{ff} (26)	1.25	181.52587(2)	$1.988(12)\ 10^{-23}$	1.016
	1.48	181.52585(2)	$2.054(12)\ 10^{-23}$	1.050

* Ratio between the corresponding line intensity and the one obtained for R=0 mm.
Note: Between parenthesis is 1 SD in unit of the last quoted digit.

Table 3: Effect on line positions and intensities of the line $P_{ff}(7)$, when one applies a single spectrum fitting procedure to spectra 1-5, with the radius of the beam fixed at 0 mm (no optical weighting), at 1.25 mm (estimated by the SOLEMIO and SRW models), or at values calculated by Eq. (2) (retained effective values).

	R (mm)	Position (cm^{-1})	Line intensity ($cm.molecule^{-1}$)	Ratio *
Spectrum 1	0	100.95941(2)	$2.625(157)\ 10^{-23}$	--
	1.25	100.95941(2)	$2.699(139)\ 10^{-23}$	1.028
	1.83	100.95942(3)	$2.937(138)\ 10^{-23}$	1.119
Spectrum 2	0	100.95942(2)	$2.390(80)\ 10^{-23}$	--
	1.25	100.95942(2)	$2.452(82)\ 10^{-23}$	1.026
	1.83	100.95942(2)	$2.650(75)\ 10^{-23}$	1.109
Spectrum 3	0	100.95942(1)	$2.598(51)\ 10^{-23}$	--
	1.25	100.95942(1)	$2.638(50)\ 10^{-23}$	1.015
	1.83	100.95942(1)	$2.775(54)\ 10^{-23}$	1.068
Spectrum 4	0	100.95938(1)	$2.568(40)\ 10^{-23}$	--
	1.25	100.95938(1)	$2.581(40)\ 10^{-23}$	1.005
	1.83	100.95938(2)	$2.635(40)\ 10^{-23}$	1.026
Spectrum 5	0	100.95936(2)	$2.557(36)\ 10^{-23}$	--
	1.25	100.95936(2)	$2.563(33)\ 10^{-23}$	1.002
	1.83	100.95936(2)	$2.589(34)\ 10^{-23}$	1.010

* Ratio between the corresponding line intensity and the one obtained for R=0 mm.
Note: Between parenthesis is 1 SD in unit of the last quoted digit.

Table 4: Line positions and intensities obtained for the $\nu_5^1 - \nu_4^1$ band of the $^{12}C_2H_2$ molecule and comparison with CDMS data. [a]

Line	σ_{obs}	$\sigma_{[10,11]}$	dif	S_{obs}	S_{calc}	%	$S_{[10,11]}$	r_{obs}	r_{calc}	$\lvert R\rvert^2_{obs}$
Pff22	65.86011	65.86002	0.09	8.744E-24	8.862E-24	1.4	8.844E-24	0.989	1.002	2.596
Pee22	66.33437	66.33427	0.10	3.023E-24	3.031E-24	0.3	3.026E-24	0.999	1.002	2.623
Pff20	70.51587	70.51583	0.04	1.365E-23	1.495E-23	9.5	1.492E-23	0.915	1.002	2.402
Pee20	70.92598	70.92597	0.01	5.305E-24	5.090E-24	-4.0	5.080E-24	1.044	1.002	2.741
Pff19	72.84709	72.84678	0.31	6.660E-24	6.319E-24	-5.1	6.307E-24	1.056	1.002	2.773
Pee19	73.22645	73.22643	0.02	2.050E-23	1.933E-23	-5.7	1.929E-23	1.063	1.002	2.791
Pff18	75.17964	75.17970	-0.06	2.227E-23	2.365E-23	6.2	2.360E-23	0.944	1.002	2.477
Pff17	77.51457	77.51454	0.03	9.573E-24	9.673E-24	1.0	9.655E-24	0.992	1.002	2.603
Pee17	77.83635	77.83635	-0.00	3.019E-23	2.946E-23	-2.4	2.941E-23	1.027	1.002	2.695
Pff16	79.85128	79.85127	0.01	3.318E-23	3.502E-23	5.5	3.496E-23	0.949	1.002	2.492
Pee16	80.14571	80.14572	-0.01	1.161E-23	1.183E-23	1.9	1.181E-23	0.983	1.002	2.581
Pff15	82.18987	82.18985	0.02	1.325E-23	1.384E-23	4.5	1.382E-23	0.959	1.002	2.517
Pee15	82.45800	82.45799	0.01	4.065E-23	4.204E-23	3.4	4.197E-23	0.969	1.002	2.543
Pff14	84.53025	84.53021	0.04	4.721E-23	4.842E-23	2.6	4.833E-23	0.977	1.002	2.565
Pee14	84.77308	84.77310	-0.02	1.530E-23	1.631E-23	6.6	1.628E-23	0.940	1.002	2.467
Pff13	86.87235	86.87234	0.01	1.838E-23	1.847E-23	0.5	1.844E-23	0.997	1.002	2.617
Pee13	87.09103	87.09101	0.02	5.533E-23	5.593E-23	1.1	5.583E-23	0.991	1.002	2.602
Pff12	89.21621	89.21617	0.04	6.040E-23	6.225E-23	3.1	6.213E-23	0.972	1.002	2.553
Pee12	89.41168	89.41169	-0.01	2.084E-23	2.091E-23	0.3	2.087E-23	0.999	1.002	2.622
Pff11	91.56165	91.56168	-0.03	2.196E-23	2.284E-23	4.0	2.280E-23	0.963	1.002	2.530
Pee11	91.73510	91.73509	0.01	6.844E-23	6.897E-23	0.8	6.884E-23	0.994	1.002	2.610
Pff10	93.90882	93.90881	0.01	7.057E-23	7.380E-23	4.6	7.366E-23	0.958	1.002	2.515
Pee10	94.06119	94.06117	0.02	2.467E-23	2.475E-23	0.3	2.470E-23	0.999	1.002	2.623
Pff 9	96.25753	96.25752	0.01	2.533E-23	2.589E-23	2.2	2.585E-23	0.980	1.002	2.573
Pee 9	96.38991	96.38988	0.03	7.450E-23	7.803E-23	4.7	7.789E-23	0.956	1.002	2.511
Pff 8	98.60777	98.60778	-0.01	7.938E-23	7.965E-23	0.3	7.950E-23	0.998	1.002	2.622
Pee 8	98.72121	98.72120	0.01	2.731E-23	2.665E-23	-2.4	2.660E-23	1.027	1.002	2.695
Pff 7	100.95955	100.95954	0.01	2.638E-23	2.643E-23	0.2	2.638E-23	1.000	1.002	2.626
Pee 7	101.05506	101.05507	-0.01	8.031E-23	7.952E-23	-1.0	7.937E-23	1.012	1.002	2.657
Pff 6	103.31275	103.31275	-0.00	7.577E-23	7.612E-23	0.5	7.600E-23	0.997	1.002	2.618
Pee 6	103.39147	103.39145	0.02	2.582E-23	2.543E-23	-1.5	2.539E-23	1.017	1.002	2.670
Pee 5	105.73031	105.73032	-0.01	7.147E-23	6.995E-23	-2.1	6.983E-23	1.023	1.002	2.687
Pff 4	108.02339	108.02339	-0.00	5.978E-23	6.008E-23	0.5	5.996E-23	0.997	1.002	2.618
Pee 4	108.07161	108.07161	-0.00	1.988E-23	2.005E-23	0.8	2.001E-23	0.994	1.002	2.608
Pff 3	110.38074	110.38073	0.01	1.467E-23	1.548E-23	5.5	1.546E-23	0.949	1.001	2.492
Pee 3	110.41532	110.41531	0.01	4.682E-23	4.648E-23	-0.7	4.641E-23	1.009	1.002	2.649
Pff 2	112.73939	112.73937	0.02	2.708E-23	2.806E-23	3.6	2.801E-23	0.967	1.002	2.538
Pee 2	112.76131	112.76135	-0.04	8.944E-24	9.361E-24	4.7	9.343E-24	0.957	1.002	2.514
Qef10	117.00834	117.00855	-0.21	1.012E-24	1.171E-24	15.7	2.095E-24	0.483	0.559	1.268
Qef 9	117.09090	117.09062	0.28	4.766E-25	5.462E-25	14.6	8.672E-25	0.550	0.630	1.443
Qef 8	117.16421	117.16450	-0.29	2.268E-24	2.253E-24	-0.7	3.229E-24	0.702	0.698	1.844
Qef 6	117.28777	117.28772	0.05	3.817E-24	4.119E-24	7.9	5.038E-24	0.758	0.818	1.989
Qef 5	117.33688	117.33702	-0.14	1.894E-24	1.852E-24	-2.2	2.133E-24	0.888	0.868	2.332
Qef 4	117.37814	117.37813	0.01	7.166E-24	7.586E-24	5.9	8.321E-24	0.861	0.912	2.261
Qef 3	117.41104	117.41101	0.03	3.519E-24	3.568E-24	1.4	3.766E-24	0.934	0.947	2.453
Qef 2	117.43568	117.43568	-0.00	1.611E-23	1.629E-23	1.1	1.671E-23	0.964	0.975	2.531
Qef 1	117.45214	117.45213	0.01	9.972E-23	1.019E-23	2.1	1.026E-23	0.972	0.993	2.551
Qfe 1	117.47199	117.47199	-0.00	2.991E-23	3.058E-23	2.2	3.080E-23	0.971	0.993	2.550
Qfe 2	117.49522	117.49526	-0.04	5.174E-24	5.435E-24	5.0	5.577E-24	0.928	0.975	2.436
Qfe 3	117.53015	117.53015	-0.00	1.066E-23	1.073E-23	0.6	1.132E-23	0.942	0.948	2.472
Qfe 4	117.57663	117.57668	-0.05	2.325E-24	2.538E-24	9.2	2.783E-24	0.835	0.912	2.193
Qfe 5	117.63479	117.63483	-0.04	5.829E-24	5.585E-24	-4.2	6.432E-24	0.906	0.868	2.380
Qfe 6	117.70469	117.70460	0.09	1.428E-24	1.383E-24	-3.1	1.692E-24	0.844	0.817	2.216
Qfe 7	117.78596	117.78600	-0.04	3.226E-24	3.087E-24	-4.3	4.059E-24	0.795	0.761	2.087
Qfe 8	117.87837	117.87900	-0.63	7.883E-25	7.605E-25	-3.5	1.090E-25	0.723	0.698	1.899
Qfe10	118.09921	118.09983	-0.62	4.048E-25	3.979E-25	-1.7	7.117E-25	0.569	0.559	1.493
Qfe11	118.22783	118.22763	0.20	8.287E-25	8.369E-25	1.0	1.722E-25	0.481	0.486	1.264
Ree 1	122.16829	122.16830	-0.01	3.180E-23	3.303E-23	3.9	3.297E-23	0.965	1.002	2.532
Rff 1	122.18598	122.18603	-0.05	1.054E-23	1.101E-23	4.5	1.099E-23	0.959	1.002	2.517
Ree 2	124.52554	124.52554	-0.00	1.957E-23	1.977E-23	1.0	1.974E-23	0.991	1.002	2.603
Rff 2	124.55054	124.55053	0.01	5.976E-23	5.933E-23	-0.7	5.923E-23	1.009	1.002	2.649
Ree 3	126.88489	126.88489	-0.00	8.586E-23	8.327E-23	-3.0	8.312E-23	1.033	1.002	2.712
Rff 3	126.91607	126.91608	-0.01	2.777E-23	2.776E-23	-0.0	2.771E-23	1.002	1.002	2.631

Table 4: (continued)

Line	σ_{obs}	$\sigma_{[10,11]}$	dif	S_{obs}	S_{calc}	%	$S_{[10,11]}$	r_{obs}	r_{calc}	$\lvert R\rvert^2_{obs}$
Ree 4	129.24632	129.24632	-0.00	3.581E-23	3.504E-23	-2.2	3.497E-23	1.024	1.002	2.689
Rff 4	129.28264	129.28264	-0.00	1.096E-22	1.051E-22	-4.1	1.049E-22	1.045	1.002	2.743
Ree 5	131.60979	131.60980	-0.01	1.272E-22	1.245E-22	-2.2	1.242E-22	1.024	1.002	2.688
Rff 5	131.65018	131.65017	0.01	4.261E-23	4.148E-23	-2.7	4.140E-23	1.029	1.002	2.703
Ree 6	133.97527	133.97527	-0.00	4.751E-23	4.694E-23	-1.2	4.685E-23	1.014	1.002	2.662
Rff 6	134.01866	134.01864	0.02	1.455E-22	1.407E-22	-3.3	1.405E-22	1.036	1.002	2.719
Ree 7	136.34272	136.34272	-0.00	1.566E-22	1.538E-22	-1.8	1.536E-22	1.020	1.002	2.678
Rff 7	136.38800	136.38801	-0.01	5.242E-23	5.123E-23	-2.3	5.114E-23	1.025	1.002	2.691
Ree 8	138.71208	138.71210	-0.02	5.470E-23	5.439E-23	-0.6	5.430E-23	1.007	1.002	2.645
Rff 8	138.75822	138.75823	-0.01	1.709E-22	1.630E-22	-4.6	1.627E-22	1.050	1.002	2.758
Ree 9	141.08334	141.08336	-0.02	1.715E-22	1.688E-22	-1.6	1.685E-22	1.018	1.002	2.673
Rff 9	141.12925	141.12927	-0.02	5.754E-23	5.617E-23	-2.4	5.606E-23	1.026	1.002	2.695
Ree10	143.45645	143.45648	-0.03	5.751E-23	5.688E-23	-1.1	5.679E-23	1.013	1.002	2.659
Rff10	143.50110	143.50109	0.01	1.826E-22	1.703E-22	-6.7	1.700E-22	1.074	1.002	2.821
Ree11	145.83140	145.83141	-0.01	1.746E-22	1.691E-22	-3.2	1.687E-22	1.035	1.002	2.717
Rff11	145.87364	145.87366	-0.02	5.805E-23	5.619E-23	-3.2	5.608E-23	1.035	1.002	2.718
Ree12	148.20810	148.20813	-0.03	5.506E-23	5.475E-23	-0.6	5.465E-23	1.008	1.002	2.645
Rff12	148.24693	148.24693	-0.00	1.729E-22	1.637E-22	-5.3	1.634E-22	1.058	1.002	2.779
Ree13	150.58656	150.58659	-0.03	1.646E-22	1.567E-22	-4.8	1.565E-22	1.052	1.001	2.762
Rff13	150.62084	150.62086	-0.02	5.470E-23	5.203E-23	-4.9	5.193E-23	1.053	1.002	2.765
Ree14	152.96671	152.96675	-0.04	4.879E-23	4.901E-23	0.5	4.892E-23	0.997	1.002	2.618
Rff14	152.99540	152.99543	-0.03	1.575E-22	1.463E-22	-7.1	1.460E-22	1.079	1.002	2.832
Ree15	155.34856	155.34858	-0.02	1.414E-22	1.357E-22	-4.0	1.354E-22	1.044	1.002	2.741
Rff15	155.37056	155.37059	-0.03	4.954E-23	4.496E-23	-9.3	4.488E-23	1.104	1.002	2.898
Ree16	157.73201	157.73204	-0.03	4.210E-23	4.109E-23	-2.4	4.100E-23	1.027	1.002	2.696
Rff16	157.74628	157.74630	-0.02	1.276E-22	1.224E-22	-4.0	1.222E-22	1.044	1.002	2.742
Ree17	160.11707	160.11711	-0.04	1.096E-22	1.102E-22	0.6	1.100E-22	0.996	1.002	2.616
Rff17	160.12250	160.12254	-0.04	3.918E-23	3.646E-23	-6.9	3.639E-23	1.077	1.002	2.827
Rff18	162.49921	162.49925	-0.04	1.002E-23	9.628E-23	-3.9	9.611E-23	1.043	1.002	2.737
Ree18	162.50370	162.50373	-0.03	3.364E-23	3.237E-23	-3.8	3.232E-23	1.041	1.002	2.733
Rff19	164.87636	164.87641	-0.05	2.784E-23	2.784E-23	0.0	2.779E-23	1.002	1.002	2.631
Ree19	164.89182	164.89188	-0.06	8.744E-23	8.433E-23	-3.6	8.419E-23	1.039	1.002	2.727
Rff20	167.25394	167.25399	-0.05	7.396E-23	7.141E-23	-3.5	7.127E-23	1.038	1.002	2.724
Ree20	167.28147	167.28152	-0.05	2.413E-23	2.406E-23	-0.3	2.402E-23	1.005	1.002	2.638
Rff21	169.63189	169.63194	-0.05	2.119E-23	2.007E-23	-5.3	2.003E-23	1.058	1.002	2.778
Ree21	169.67256	169.67261	-0.05	6.041E-23	6.094E-23	0.9	6.083E-23	0.993	1.002	2.608
Rff22	172.01014	172.01022	-0.08	5.220E-23	5.005E-23	-4.1	4.996E-23	1.045	1.002	2.743
Ree22	172.06506	172.06512	-0.06	1.634E-23	1.691E-23	3.5	1.688E-23	0.968	1.002	2.542
Rff23	174.38872	174.38881	-0.09	1.322E-23	1.368E-23	3.5	1.365E-23	0.968	1.002	2.542
Ree23	174.45896	174.45902	-0.06	4.022E-23	4.164E-23	3.5	4.157E-23	0.968	1.002	2.540
Rff24	176.76757	176.76767	-0.10	3.313E-23	3.321E-23	0.2	3.315E-23	0.999	1.002	2.624
Ree24	176.85424	176.85427	-0.03	1.082E-23	1.125E-23	4.0	1.123E-23	0.963	1.002	2.531
Rff25	179.14663	179.14677	-0.14	8.560E-24	8.836E-24	3.2	8.820E-24	0.971	1.002	2.548
Ree25	179.25078	179.25084	-0.06	2.630E-23	2.698E-23	2.6	2.693E-23	0.977	1.002	2.565
Rff26	181.52594	181.52606	-0.12	2.041E-23	2.089E-23	2.3	2.084E-23	0.979	1.002	2.571
Ree26	181.64863	181.64868	-0.05	6.699E-24	7.093E-24	5.9	7.080E-24	0.946	1.002	2.484
Rff27	183.90541	183.90552	-0.11	5.284E-24	5.411E-24	2.4	5.402E-24	0.978	1.002	2.568
Ree27	184.04772	184.04778	-0.06	1.562E-23	1.657E-23	6.1	1.654E-23	0.944	1.002	2.479
Rff28	186.28493	186.28511	-0.18	1.157E-23	1.246E-23	7.7	1.244E-23	0.930	1.002	2.442
Ree28	186.44803	186.44809	-0.06	3.962E-24	4.246E-24	7.2	4.238E-24	0.935	1.002	2.455
Rff29	188.66467	188.66479	-0.12	2.887E-24	3.147E-24	9.0	3.141E-24	0.919	1.002	2.413
Ree29	188.84956	188.84958	-0.02	8.801E-24	9.664E-24	9.8	9.648E-24	0.912	1.002	2.395
Rff30	191.04437	191.04454	-0.17	6.814E-24	7.061E-24	3.6	7.048E-24	0.967	1.002	2.538
Ree30	191.25211	191.25221	-0.10	2.344E-24	2.414E-24	3.0	2.409E-24	0.973	1.002	2.554

[a] The quoted line positions (in cm^{-1}) σ_{obs} and $\sigma_{[10,11]}$ are those measured respectively in this work and in Refs. [10,11]. The dif column is the difference in 10^{-3} cm^{-1} between the line positions obtained in this work, and those deduced from Ref. [10] and given in CDMS [11]. S_{obs} and S_{calc} are measured and calculated intensities, respectively, for pure $^{12}C_2H_2$ (i.e., for a sample containing 100% of $^{12}C_2H_2$), in cm $molecule^{-1}$ at 296 K. The column noted % is equal to $100 \times (S_{calc} - S_{obs}) / S_{obs}$. $S_{[10,11]}$ are the calculated intensities in cm $molecule^{-1}$ at 296 K given in Ref. [11] and coming from Ref. [10]. The two following columns noted r_{obs} and r_{calc} are the ratios $S_{obs} / S_{[10,11]}$ and $S_{calc} / S_{[10,11]}$. $|R|^2_{obs}$ is the experimental transition dipole moment squared value, in 10^{-3} D^2 (1 D = 3.33546×10^{-30} C m), deduced from S_{obs} using Eqs. (3-7) with g_v equal to 1 (see text).

Figure 1: Overview of the weak *Q*-branches of the $\nu_5^1 - \nu_4^1$ band around 117.5 cm^{-1} on spectrum 4 (see Table1).

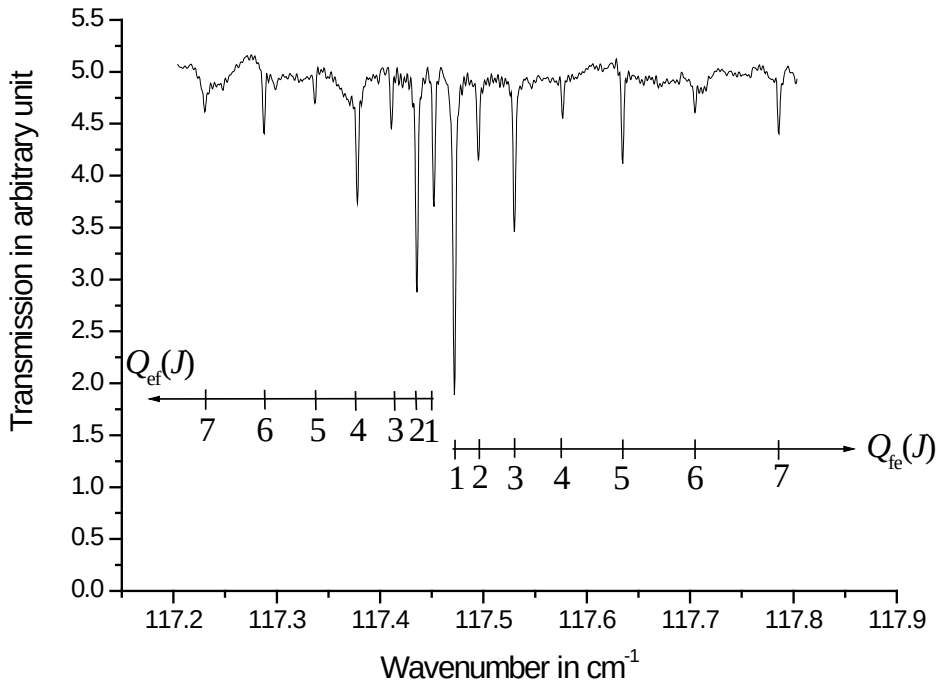

Figure 2: Estimation of the fitting parameter R_{eff}. The three stars are estimations of the size of the beam obtained using the SOLEMIO and SRW models at 10, 100 and 1000 cm^{-1}. The values of R_{eff} are indicated by solid symbols for acetylene transitions and by open symbols for water transitions. For spectrum 1, 2, 3, and 4, squares, triangles, circles, and upside down triangles have been respectively used.

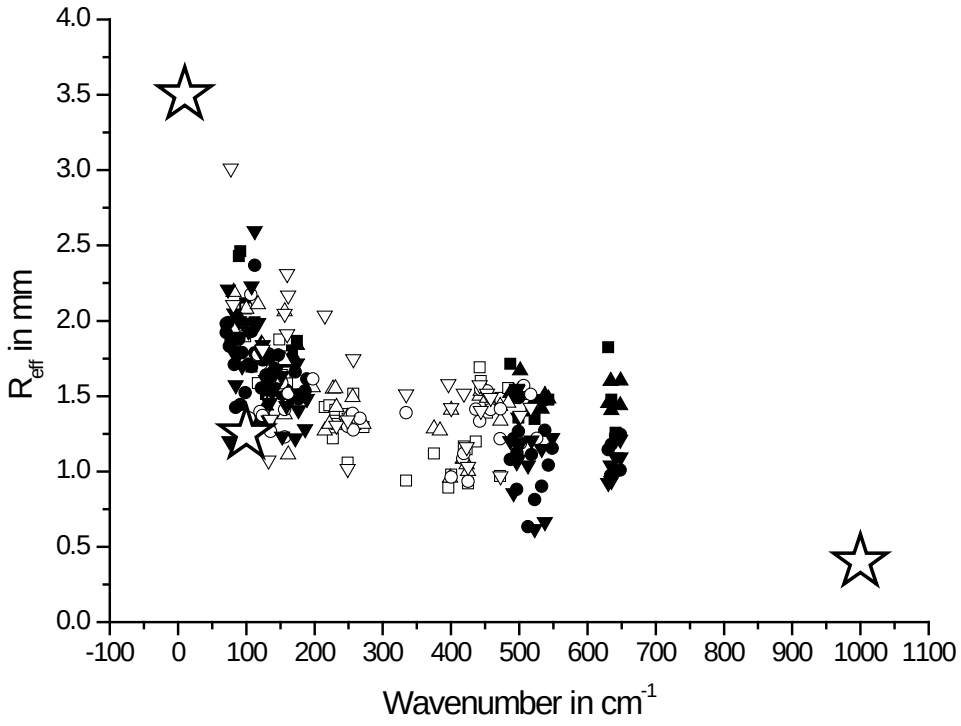

Figure 3: Apparatus functions calculated around 80 (a), 100 (b) and 180 cm^{-1} (c), for various optical weightings. The continuous line represents the apparatus function without optical weighting (R=0 mm), whereas the dash and dot lines correspond respectively to an optical weighting using R=1.25 mm (estimated by the SOLEMIO and SRW models) and R deduced from Eq. (2) (see Table 2).

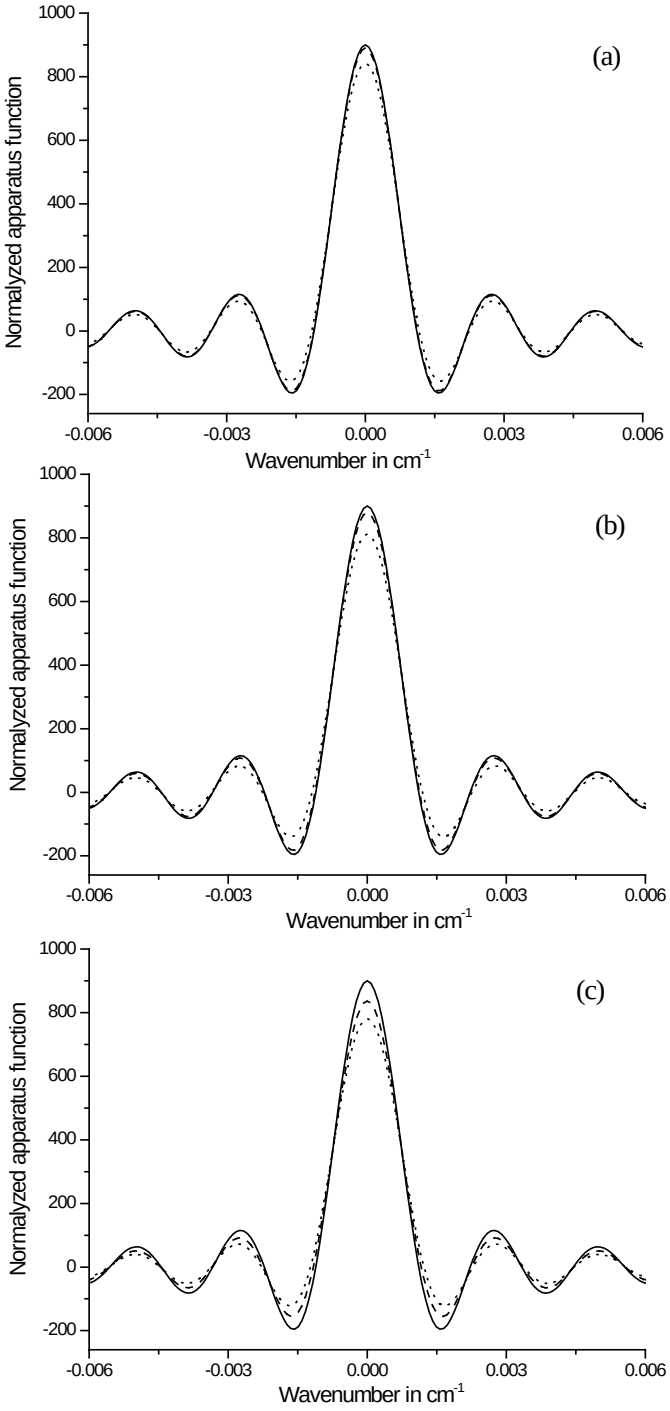

Figure 4: Residuals of a multispectrum fitting of the R_{ff} (26) line located around 181.5 cm^{-1}. The residuals are those obtained with no optical weighting (a), using R = 1.25 mm (b), and R = 1.48 mm (c). The experimental transmission is plotted. The sidelobes of the apparatus function are clearly visible and are well reproduced by the adjustments (differences can not be distinguished). The absence of systematic signature in the residuals of the body of the line (c), contrary to what is observed on plots (a) and (b), shows that our model of apparatus function is efficient and precise enough.

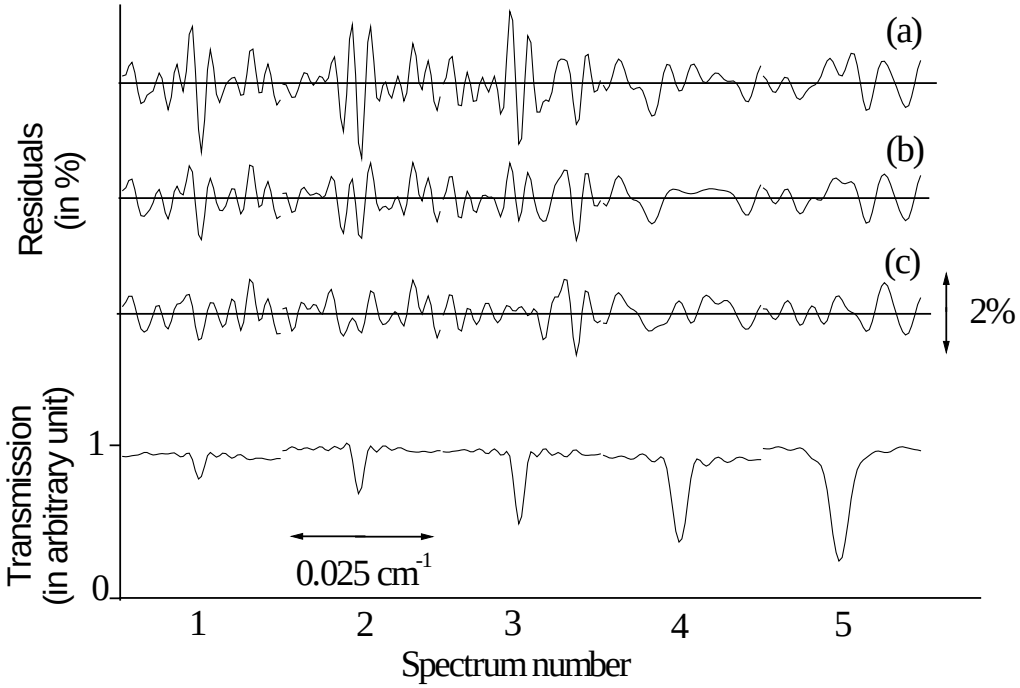

Figure 5: Transition dipole moment squared $|R|^2$ for the lines of the $\nu_5{}^1 - \nu_4{}^1$ band of acetylene $^{12}C_2H_2$. Solid symbols represent the P_{ee}, R_{ee} and Q_{fe} branches, whereas the open ones are for the P_{ff}, R_{ff} and Q_{ef} branches. Triangles represent both the *R*- and *P*-branches, whereas the square symbols are for the *Q*-branches. The continuous lines represent the calculation using Eqs. (6-7) together with the $|R_0|^2$ and $A_2{}^Q$ values given in the text.